Modeling Demands for Nanoscale Devices

(Invited Paper)

M. Pourfath, V. Sverdlov, and S. Selberherr
Institute for Microelectronics, TU Wien, 1040 Vienna, Austria
Email: {pourfath|sverdlov|selberherr}@iue.tuwien.ac.at

Abstract

With the progress of miniaturization the size of electronic devices is presently scaling down into the nanometer region, where quantum mechanical effects play an important role. Appropriate technology computer-aided design tools are essential to explore the physics of nanoscale devices and to find methods to optimize their functionality and performance. In this work we review the approaches to quantum mechanical modeling of carrier transport in nanoscale electronic devices. Numerical analyses for graphene nanoribbons are presented as a case study.

I. Introduction

For more than four decades the progress of integrated circuit technology has been based upon the down-scaling of Si-MOSFETs. The number of devices contained on a single chip has approximately doubled every three years. The continued miniaturization of Si integrated devices has approached the nanometer region. Novel structures, such as multiple gate MOSFETs, and novel materials beyond Si, such as compound semiconductors and graphene, are expected to be utilized to meet the requirements for further scaling [1]. On the other hand novel devices based on quantum mechanical effects, such as tunneling FETs [2], have been introduced in recent years.

Rapid changes in technological solutions and device architectures can be anticipated by employing technology computer-aided design (TCAD) tools which assist in device development and engineering at practically all stages from process definition to circuit optimization. TCAD tools help to reduce costs of research and development of new processes and devices [3]. The classical drift-diffusion model of carrier transport in electronic device has been widely employed in TCAD tools. However, the concern is increasing about how quantum effects will impact electronic device operation as down-scaling of electronic devices continues along the road-map and, in addition, the demand for numerical analysis and optimization of novel devices which are based on quantum effects is increasing. Therefore, modern TCAD tools based on quantum transport models are indeed required [4].

In Section II different semi-classical and quantum mechanical transport models are briefly introduced. In Section III the non-equilibrium Green's function fornalism (NEGF), which is widely used for the analysis of nanoscale devices, is discussed in moderate detail. In Section IV the NEGF method is applied to study graphene nanoribbons. Finally, conclusions are drawn in Section V.

II. The Hierarchy of Transport Models

Table I sketches the hierarchy of different transport models for device modeling. There are two fundamental equations for semi-classical device simulation, the Poisson equation and the Boltzmann equation. While the Poisson equation takes care of the electrostatic description of any device structure, the Boltzmann equation describes the propagation of a particle distribution function $f(\mathbf{r}, \mathbf{k}, t)$ within the device. These two equations have to be solved in a self-consistent manner and can be exploited as a reference for numerous models which are derived from the Boltzmann transport equation [5]. The distribution function $f(\mathbf{r}, \mathbf{k}, t)$ is a classical concept which holds, when the characteristic length of the device is much larger than the De Broglie wavelength of carriers, $L \gg \lambda$.

A direct solution of the Boltzmann equation is possible only for a few rather pathological cases. The Boltzmann equation can be solved by using the Monte Carlo method [6]. An approximate solution can be obtained by expressing the distribution function as a series expansion which leads to the spherical harmonics approach [7]. The method of moments is also a very efficient way to derive approximate solutions of the Boltzmann transport equation [5]. By multiplying the Boltzmann transport equation with a set of weight functions and integrating over k-space one can deduce a set of balance and flux equations coupled with the Poisson equation. Via this formalism an arbitrary number of equations can be generated. One has to truncate the equation system at a certain point and complete the system by an additional condition [8]. For example, the drift-diffusion model can be gained by assuming thermal equilibrium between the charge carriers and the lattice [5]. However, when the device size is scaled down, the carriers' non-equilibrium properties caused by a high electric field become important. The hydrodynamic transport model addresses this issue by assuming a heated Maxwellian distribution for the carriers [9].

The Poisson equation and the Schrödinger equation are the basis of all quantum transport models. However, solving the Schrödinger equation for a many particle system is very difficult. To address the many body problem different techniques and methods have been introduced. Among them the NEGF formalism, see Section III, appears to be appropriate for nanoscale devices [10, 11]. In coordinate representation the Green's function, $G(\mathbf{r_1}, t_1; \mathbf{r_2}, t_2)$, depends on two position arguments $\mathbf{r_1}, \mathbf{r_2}$ and two time arguments t_1, t_2, representing the non-locality in space and time.

978-1-4244-7870-5/10/$26.00 ©2010 IEEE

TABLE I
The hierarchy of semi-classical and quantum transport models.

Transport Regime	Quantum Mechanical $L \sim \lambda$			Semi-classical $L \gg \lambda$		
Fundamental Equation	Schrödinger			Boltzmann		
Transport Model	Non-equlibrium Green's Function	Wigner	Quantum Corrected Boltzmann Quantum Hydrodynamics	Boltzmann (Monte Carlo)	Hydrodynamics	Drift-Diffusion

Device Characteristic Length (L) ⟶

The equation of motion for the Green's function is given by the integro-differential Dyson equation [12]. On the other hand, starting from the Dyson equation, the quantum Boltzmann equation can be derived [13]. When independent variables are changed to the center of mass coordinates $(\mathbf{r}, t) = (\mathbf{r}_1 + \mathbf{r}_2, t_1 + t_2)/2$ and the relative coordinates $(\mathbf{u}, \tau) = (\mathbf{r}_1 - \mathbf{r}_2, t_1 - t_2)$, a quantum mechanical distribution function $G(\mathbf{k}, \omega, \mathbf{r}, t)$ is defined as the Fourier transform of $G(\mathbf{u}, \tau, \mathbf{r}, t)$ with respect to the relative coordinates. The quantum Boltzmann equation is in fact a kinetic differential equation for the Green's function [13].

The Wigner distribution function is defined as the energy integral of the Green's function [14]. A transport equation for the Wigner distribution function including scattering effects can be obtained [15]. A practically used approximation to incorporate realistic scattering processes into the Wigner equation is to utilize the Boltzmann scattering operator [16], or by an even simpler scheme such as the relaxation time approximation[17]. Under this approximation, quantum mechanical collisional effects, for example, collisional energy broadening [18], are neglected. One can continue by rewriting the Wigner equation in the form of a modified Boltzmann equation with additional terms including quantum correction [14]. Based on this equation the quantum corrected Boltzmann equation, the quantum hydrodynamic, and the density gradient approximation can be achieved [19].

III. The non-Equilibrium Green's Function Formalism

As discussed in the previous section, the NEGF method appears to be the most appropriate model for nanoscale devices [11, 20, 21]. In this formalism quantum effects, such as tunneling, size quantization, and interference are considered in the treatment of carriers. Quantum mechanical collisional effects in the scattering of carriers, such as collisional energy broadening, are also properly modeled. This method has been successfully applied to study molecular devices [22–24], Si-MOSFETs [25–28], nanowires [29–32] CNTs [33–37], GNRs [38–41], and spin transport [42–44]

The NEGF formalism initiated by Schwinger, Kadanoff and Baym [45], and Keldysh [12] allows to study the time evolution of a many-particle quantum system. The many-particle information about the system is cast into self-energies, which are part of the equations of motion. A perturbation expansion of the Green's functions is the key to approximate the self-energies. Green's functions enable a powerful technique to evaluate the properties of a many-body system both in thermodynamic equilibrium and non-equilibrium situations [46].

Four types of Green's functions are defined as the non-equilibrium statistical ensemble averages of the single particle correlation operator [12]. The greater Green's function $G^>$ and the lesser Green's function $G^<$ deal with the statistics of carriers. The retarded Green's function G^R and the advanced Green's function G^A describe the dynamics of carriers.

$$\begin{aligned} G^>(1,2) &= -i\hbar^{-1}\langle\hat{\psi}(1)\hat{\psi}^\dagger(2)\rangle & G^\mathrm{R}(1,2) &= \theta(t_1 - t_2)[G^>(1,2) - G^<(1,2)] \\ G^<(1,2) &= +i\hbar^{-1}\langle\hat{\psi}^\dagger(2)\hat{\psi}(1)\rangle & G^\mathrm{A}(1,2) &= \theta(t_2 - t_1)[G^<(1,2) - G^>(1,2)] \end{aligned} \tag{1}$$

The abbreviation $1 \equiv (\mathbf{r_1}, t_1)$ is used, $\langle \ldots \rangle$ is the statistical average with respect to the density operator, $\theta(t)$ is the unit step function, $\hat{\psi}^\dagger(\mathbf{r_1}, t_1)$ and $\hat{\psi}(\mathbf{r_1}, t_1)$ are the field operators creating or destroying a particle at point $(\mathbf{r_1}, t_1)$ in space-time, respectively. The Green's functions are all correlation functions. For example, $G^>$ relates the field operator $\hat{\psi}$ of the particle at point $(\mathbf{r_1}, t_1)$ in space-time to the conjugate field operator $\hat{\psi}^\dagger$ at another point $(\mathbf{r_2}, t_2)$.

Under steady state condition the Green's functions depend only on time differences. One usually Fourier transforms the time difference coordinate, $\tau = t_1 - t_2$, to energy. For example, the lesser Green's function is transformed as $G^<(1,2) \equiv G^<(\mathbf{r_1}, \mathbf{r_2}; E) = \int (d\tau/\hbar) e^{iE\tau/\hbar} G^<(\mathbf{r_1}, \mathbf{r_2}; \tau)$. Under this condition the equation of motion for the Green's functions can be written as [10]:

$$[E - H]\, G^{\mathrm{R,A}}(1,2) - \int d3\, \Sigma^{\mathrm{R,A}}(1,3) G^{\mathrm{r,a}}(3,2) = \delta_{1,2} \qquad G^{\lessgtr}(1,2) = \int d3 \int d4 G^\mathrm{R}(1,3) \Sigma^{\lessgtr}(3,4) G^\mathrm{A}(4,2) \tag{2}$$

where H is the single-particle Hamiltonian operator, and Σ^R, $\Sigma^<$, and $\Sigma^>$ are the retarded, lesser, and greater self-energies, respectively.

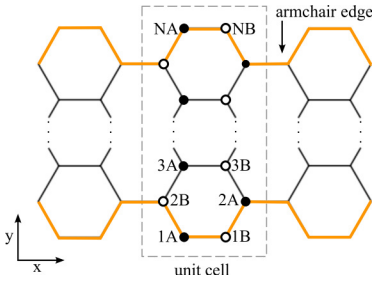

Fig. 1. The structure of a GNR with armchair edges along the transport direction. Each unit cell consists of N numbers of A and B sublattices.

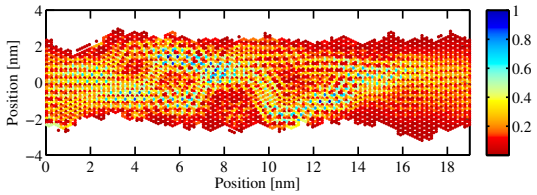

Fig. 2. Spatial distribution of the normalized current amplitude along a GNR with line-edge roughness. The ribbon's length is 19nm and the width is 5nm. An exponential auto-correlation for line-edge roughness has been assumed. The roughness is described by a correlation length of $L_m = 3\text{nm}$ and an amplitude of $\Delta_m = 2a_{\text{cc}}$.

IV. Analysis of Graphene Nanoribbons

Graphene, a one-atomic carbon sheet with a honeycomb structure, has attracted significant attention due to its unique physical properties [47]. This material shows an extraordinarily high carrier mobility of more than $2\times10^5\text{cm}^2/\text{Vs}$ [48] and is considered a major candidate for a future channel material for high performance transistors [49, 50]. To induce an electronic bandgap, a graphene sheet can be patterned into narrow ribbons [51]. In order to obtain an energy bandgap larger than 0.1eV, which is essential for electronic applications, the width of the GNR must be scaled below 10nm [52]. In this regime line-edge roughness is the dominant scattering mechanism [53]. The tight-binding model for GNRs [51], which is used in this work, is described first. Applying this model, the effect of linde-edge roughness is studied next.

A. Tight-Binding Model

The structure of graphene consists of two types of sublattices A and B, see Fig. 1. In graphene three σ bonds hybridize in an sp^2 configuration, whereas the other $2p_z$ orbital which is perpendicular to the graphene layer, forms π covalent bonds [54]. Each atom in an sp^2-coordination has three nearest neighbors, located $a_{\text{cc}} = 1.42\text{Å}$ away. It is well known that the electronic and optical properties of CNTs and GNRs are mainly determined by the π electrons [55]. To model those π electrons, a nearest neighbor tight-binding approximation has been widely used. Using this approximation the Hamiltonian can be written as:

$$H = t \sum_{\langle p,q \rangle} \left(|A_p\rangle\langle B_q| + |B_q\rangle\langle A_p| \right) \ , \tag{3}$$

where $|A_p\rangle$ and $|B_q\rangle$ are atomic wave functions of the $2p_z$ orbitals which are centered at lattice sites labeled as A_p and B_q, respectively. $\langle p, q\rangle$ represents pairs of nearest neighbor sites p and q, $t = -2.7$ eV is the transfer integral, and the on-site potential is assumed to be zero. For the structure shown in Fig. 1 the matrix elements of the Hamiltonian are non-zero for $p = q$ and $p = q \pm 1$. This atomistic model produces a matrix whose size is the total number of carbon atoms [56]. The advantage of this model is that it can describe the device in an atomistic way. In this method the effect of lattice vacancies [57], roughness [39], impurities [58], and disorder [59] can be rigorously modeled by changing the hopping parameter at respective atomic sites.

B. Line-Edge Roughness

The line-edge roughness can be perturbatively treated [53]. However, in a more accurate non-perturbative approach one can consider the roughness as a stochastic phenomenon and adapt it by removing or replacing specific carbon atoms located at the edges of the ribbon. In order to model roughness, an exponential auto-correlation function is defined as [60]:

$$c(n) = \Delta_m^2 \exp\left(-\frac{x}{L_m}\right), \quad x = n\Delta x \tag{4}$$

where Δ_m is the roughness amplitude, L_m is the correlation length, and $\Delta x = a_{\text{cc}}/2$ is the sampling interval. The stochastic roughness can be generated by applying a random phase to the power spectrum of the roughness auto-correlation in the Fourier domain and inverse Fourier transforming in order to obtain roughness in the real space domain [60]. Fig. 2 shows the spatial distribution of the current amplitude along a GNR with rough edges. Due to multiple scattering of carriers between the two rough edges, a large circulating current is present at some locations inside the channel. Furthermore, the atomistic tight-binding model can capture the granularity of the simulation domain, which is essential for narrow GNRs. To investigate the effect of roughness on the current of GNRs, one can consider the ratio of the GNR current in the presence of roughness to that of a GNR with perfect edges $R_{\text{Rough}} = I_{\text{Rough}}/I_{\text{Perfect}}$. Fig. 3-a shows R_{Rough} as a function of the roughness amplitude. As the roughness amplitude increases the current decreases. The decrease of the current can be attributed to more coherent scattering by imperfect edges and also the increase of the energy bandgaps. In fact as the roughness amplitude increases, the width of the ribbon decreases at

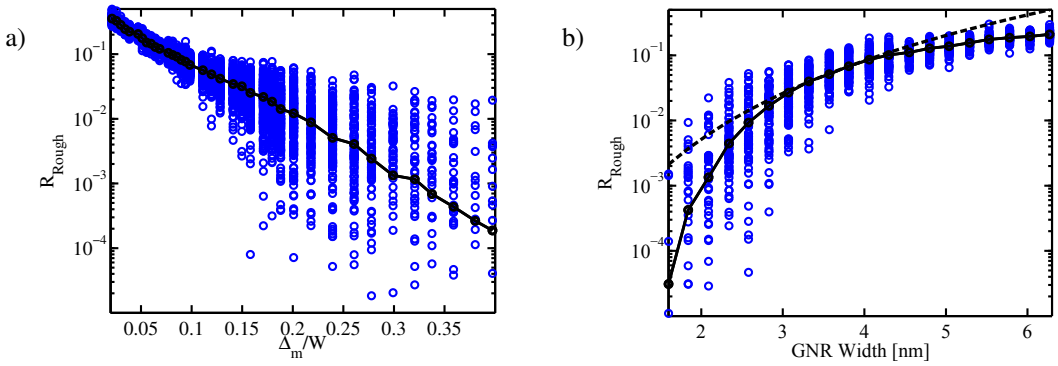

Fig. 3. a) R_{Rough} as a function of the roughness amplitude. The roughness amplitude is normalized to the GNR width. The GNR has a width of $W = 2.36\mathrm{nm}$ and a length of $L = 20\mathrm{nm}$. The correlation length of the line-edge roughness is $L_m = 3\mathrm{nm}$. b) R_{Rough} as a function of the ribbon's width. The roughness amplitude is $\Delta_m = 4a_{\mathrm{cc}}$. The dashed line shows a W^4 term for comparison with semiclassical simulations [53].

some locations. Since the energy gap is inversely proportional to the ribbon's width, the local decrease of the width results in an increase of the local energy gap, which results in an exponential decrease of the current. This behavior can not be captured by semi-classical simulations, where the mobility of GNRs due to roughness scattering is reported to be proportional to W^4 [53]; W is the width of the ribbon. This can be observed in Fig. 3-b, where R_{Rough} is shown as a function of the GNR width. The results indicate an exponential change of the current rather than a W^4 relation. The deviation is more pronounced for narrow ribbons.

V. Conclusion

A review of semi-classical and quantum mechanical transport models for the analysis of semiconductor devices is presented. The approximations and the limitations of each model are discussed. The non-equilibrium Green's function formalism provides a self-consistent approach for the analysis of nanoscale devices. In this formalism scattering processes and quantum mechanical phenomena can be rigorously modeled. As a case study we investigated the effect of line-edge roughness on the electronic properties of GNRs. An atomistic tight-binding model, which captures the granularity of the simulation domain, has been used. The results indicate the importance of employing non-continuum quantum mechanical simulations for the accurate analysis of nanoscale devices.

References

[1] International Technology Roadmap for Semiconductors - 2009 Edition, http://public.itrs.net.
[2] W. Choi *et al.*, IEEE Electron Device Lett. **28**, 743 (2007).
[3] V. Sverdlov *et al.*, Mat. Sci. Eng. R **8**, 192 (2009).
[4] V. Sverdlov *et al.*, J. Comp. Electronics **58**, 228 (2008).
[5] M. Lundstrom, *Fundamentals of Carrier Transport*, 2nd ed. (Cambridge University Press, Cambridge, 2000).
[6] C. Jacoboni *et al.*, *The Monte Carlo Method for Semiconductor Device Simulation* (Springer, Vienna, 1989).
[7] N. Goldsman *et al.*, Superlattices Microstruct. **27**, 159 (2000).
[8] C. Jungemann *et al.*, *Hierarchical Device Simulation* (Springer, Vienna, 2003).
[9] T. Grasser *et al.*, Proc. IEEE **91**, 251 (2003).
[10] R. Lake *et al.*, J. Appl. Phys. **81**, 7845 (1997).
[11] M. P. Anantram *et al.*, IEEE Trans. Electron Devices **54**, 2100 (2007).
[12] L. V. Keldysh, Soviet Phys. JETP **20**, 1018 (1965).
[13] G. D. Mahan, Physics Reports **145**, 251 (1987).
[14] E. Wigner, Phys. Rev. **40**, 749 (1932).
[15] M. Nedjalkov *et al.*, Phys. Rev. B **70**, 115319 (16pp) (2004).
[16] R. K. Mains *et al.*, J. Appl. Phys. **64**, 5041 (1988).
[17] K. L. Jensen *et al.*, J. Appl. Phys. **67**, 7602 (1990).
[18] S. Datta, Superlattices Microstruct. **28**, 253 (2000).
[19] H. Tsuchiya *et al.*, IEICE Trans. Electron. **E82-C**, 880 (1999).
[20] R. Lake *et al.*, Superlattices Microstruct. **20**, 279 (1996).
[21] G. Klimeck *et al.*, IEEE Trans. Electron Devices **54**, 2079 (2007).
[22] W. Tian *et al.*, J. Chem. Phys **109**, 2874 (1998).
[23] P. S. Damle *et al.*, Phys. Rev. B **64**, 201403 (2001).
[24] A. W. Ghosh *et al.*, Nano Lett. **4**, 565 (2004).
[25] A. Svizhenko *et al.*, J. Appl. Phys. **91**, 2343 (2002).
[26] R. Venugopal *et al.*, J. Appl. Phys. **93**, 5613 (2003).
[27] C. Rivas *et al.*, Phys. Status Solidi B **239**, 94 (2003).
[28] A. Svizhenko *et al.*, IEEE Trans. Electron Devices **50**, 1459 (2003).
[29] X. Shao *et al.*, Solid-State Electron. **49**, 1435 (2005).
[30] A. Martinez *et al.*, Physica E **37**, 168 (2006).
[31] M. Shin, IEEE Trans. Nanotechnol. **6**, 230 (2007).
[32] M. Luisier *et al.*, Phys. Rev. B **80**, 155430 (11pp) (2009).
[33] D. A. Stewart *et al.*, Phys. Rev. Lett. **93**, 107401 (2004).
[34] A. Svizhenko *et al.*, Phys. Rev. B **72**, 085430 (2005).
[35] L. Castro *et al.*, IEEE Trans. Nanotechnol. **4**, 699 (2005).
[36] M. Pourfath *et al.*, Nanotechnology **18**, 424036 (2007).
[37] S. O. Koswatta *et al.*, IEEE Trans. Electron Devices **54**, 2339 (2007).
[38] B. Obradovic *et al.*, Appl. Phys. Lett. **88**, 142102 (3pp) (2006).
[39] Y. Yoon *et al.*, Appl. Phys. Lett. **91**, 073103 (3pp) (2007).
[40] G. Fiori *et al.*, IEEE Electron Device Lett. **28**, 760 (2007).
[41] Y. Ouyang *et al.*, Appl. Phys. Lett. **92**, 243124 (3pp) (2008).
[42] Y. Sandu *et al.*, Phys. Rev. B **73**, 075313 (8pp) (2006).
[43] J. Guo *et al.*, Appl. Phys. Lett. **92**, 163109 (3pp) (2008).
[44] T. Low *et al.*, J. Appl. Phys. **104**, 094511 (10pp) (2008).
[45] L. P. Kadanoff *et al.*, *Quantum Statistical Mechanics: Green's Function Methods in Equilibrium and Non-Equilibrium Problems* (W.A. Benjamin, New York, 1962).
[46] S. Datta, *Quantum Transport: From Atoms to Transistors* (Cambridge University Press, Cambridge, 2005).
[47] A. Geim *et al.*, Nature Mater. **6**, 183 (2007).
[48] K. Bolotin *et al.*, Solid-State Commun. **146**, 351 (2008).
[49] Y.-M. Lin *et al.*, Science **327**, 661 (2010).
[50] F. Xia *et al.*, Nano Lett. **10**, 715 (2010).
[51] C. Berger *et al.*, Science **312**, 1191 (2006).
[52] M. Han *et al.*, Phys. Rev. Lett. **98**, 206805 (4pp) (2007).
[53] T. Fang *et al.*, Phys. Rev. B **78**, 205403 (8pp) (2008).
[54] R. Saito *et al.*, *Physical Properties of Carbon Nanotubes* (Imperial College Press, London, 1998).
[55] Y.-W. Son *et al.*, Nature (London) **444**, 347 (2006).
[56] J. Guo *et al.*, Intl. J. Multiscale Comput. Eng. **2**, 257 (2004).
[57] Y. Yoon *et al.*, IEEE Trans. Electron Devices **55**, 2314 (2009).
[58] N. Neophytou *et al.*, Appl. Phys. Lett. **88**, 242106 (3pp) (2006).
[59] X. Ni *et al.*, Appl. Phys. Lett. **95**, 192114 (3pp) (2009).
[60] S. M. Goodnick *et al.*, Phys. Rev. B **33**, 8171 (1985).